Results in Materials 22 (2024) 100558

Contents lists available at ScienceDirect

Results in Materials

journal homepage: www.sciencedirect.com/journal/results-in-materials

First-principles calculations to investigate the elastic, electronic, dynamical, and optical properties of cubic ZrCoAs half-Heusler semiconductor for photovoltaic applications

Lynet Allan [a,*], R.E. Mapasha [b], Winfred M. Mulwa [c], Julius M. Mwabora [a], Robinson J. Musembi [a]

[a] Department of Physics, Faculty of Science and Technology, University of Nairobi, P.O.Box 30197-00100, Nairobi, Kenya
[b] Department of Physics, University of Pretoria, Private Bag x 20, Hatfield, South Africa
[c] Department of Physics, Faculty of Science, Egerton University, P.O Box 536-20115, Egerton, Kenya

ARTICLE INFO

Keywords:
Cubic ZrCoAs
Half-Heusler semiconductor
Photovoltaic
Elastic properties
Electronic properties
Dynamical properties
Optical properties

ABSTRACT

The electronic, mechanical, elastic, dynamical, and optical properties of the ZrCoAs half-Heusler compound have been systematically investigated using the plane wave self-consistent field approach with the Perdew-Burke-Erzerhof generalized gradient approximation (GGA-PBE) exchange-correlation functional. The study includes examinations with and without spin orbit coupling (SOC) effects. Results indicate a decrease in the Kohn-Sham band gap with the inclusion of SOC effects. Electronic bandgap formation was attributed to Co 3d, Zr 3d, and As 2p for the conduction band, and Co 3d and As 2p for the valence band without SOC effects. With SOC, Co 5d, Zr 8d, and As 3p dominated the conduction band, while Co 3d and As 3p dominated the valence band. The lattice constant showed a 0. 063% decrease with the SOC effects, which is better aligned with the experimental observations. ZrCoAs demonstrated ductility, mechanical stability, and dynamical stability. The optical properties were found to be excellent for photovoltaic applications, suggesting its potential in solar energy conversion technology. This study provides valuable information on ZrCoAs and presents opportunities for its use in solar cells, optoelectronic devices, and thermoelectric applications. The material's versatility and suitability for practical applications make it a promising candidate for further exploration in renewable energy research.

1. Introduction

The global demand for sustainable and renewable energy sources has spurred extensive research in the field of photo-voltaic materials that aims to harness solar energy for power generation [1]. Among the various materials investigated, Heusler compounds have garnered significant attention due to their captivating electronic, magnetic, and thermo-electric properties [2–8]. These intermetallic compounds, named after Friedrich Heusler, exhibit a cubic structure and comprise three elements: an alkali or alkaline earth metal (A), a transition metal (B), and a metalloid (X), leading to the formation of ABX for half Heuslers and AB_2X for full Heuslers [9]. Heusler compounds have exhibited potential for use in photovoltaics, providing a unique avenue for enhancing solar energy conversion efficiency. Zirconium-based alloys, with applications ranging from automobiles to energy sectors, have gained attentions [10]. Specifically, half- Heusler compounds ZrCoY (Y═Sb, Bi) have emerged as captivating candidates for photovoltaic and thermoelectric applications due to their tunable properties [2–9].

Among the Zr-based half Heusler semiconductors, the ZrCoAs compound underscores its significance within the realm of intermetallic compounds, spotlighting its distinct electronic, magnetic, and structural attributes [11]. The potential for superconductivity of the compound has been investigated, along with its response to extreme conditions. These findings hold promise for applications in diverse fields, facilitated by advances in synthesis and characterization techniques, paving the way for potential use in quantum materials, superconducting electronics, and spintronics [11]. Despite the significant progress made in understanding half Heusler compounds [2,7,9], to the best of our knowledge, limited research has focused on the ZrCoAs compound specifically for photovoltaic applications. In this paper, we present an ab-initio study aimed at analyzing the electronic, optical, elastic, dynamical, and structural properties of the half-Heusler compound

* Corresponding author.
E-mail addresses: allanlynet254@gmail.com, allanlynet3@students.uonbi.ac.ke (L. Allan).

https://doi.org/10.1016/j.rinma.2024.100558
Received 8 November 2023; Received in revised form 9 February 2024; Accepted 7 March 2024
Available online 9 March 2024

ZrCoAs with the aim of bridging this research gap. We employ first-principles calculations to accurately determine the fundamental properties of ZrCoAs. This approach unveils key electronic properties, such as the band structure and optical absorption properties, enriching our understanding of the potential of the material as a light-harvesting medium. Furthermore, the study of elastic properties, mechanical properties, and lattice dynamics offers insight into the mechanical and dynamic stability of ZrCoAs, which are critical for the reliability and longevity of energy-harvesting devices. The investigation of ZrCoAs's properties further con-tributes to the understanding of its crystal symmetry and lattice constants, which are crucial for device optimization and design.

The objective of this study is to conduct a comprehensive analysis of the ZrCoAs half-Heusler compound, focusing on its electronic, mechanical, elastic, and optical properties with the aim of assessing the material's potential for application in solar energy conversion technology. This research seeks to contribute valuable information to the scientific understanding and advancement of sustainable energy technologies. The paper is organized as follows. Section 2 outlines the calculations made for future reference. In Section 3, we go into the details of our findings. Structural characteristics are discussed in Section 3A, while Section 3B covers the projected density of states (PDOS) and electronic band structures. The discussion of elastic constants and mechanical stability is presented in Section 3C. Section 3D explores the dynamical properties of the compounds, including phonon dispersions, followed by the analysis of the optical response of ZrCoAs in Section 3E. The summary is outlined in Section 4.

2. Calculations

To perform our calculations, we obtained the crystal structure files from the Materials Project [12]. Subsequently, the input files were generated using the Quantum Espresso tools available on the Materials Cloud platform [13]. The choice of the GGA-PBE exchange correlation functional [14] was based on previous research carried out by Allan et al. [15], where this functional demonstrated the best performance among various exchange-correlation options tested for Zr-based HH alloys. Additionally, ultra-soft non-linear core corrections [16] were used and a scalar relativistic treatment was applied to the elements Zr, Co, and As. This selection of computational methodologies improved the accuracy of the electronic structure calculations for the ZrCoAs system. A 50Ry cutoff energy was used and the integration of the Brillouin zone was performed using a Monkhorst-Pack grid with dimensions of $5 \times 5 \times 5$. The ground-state structural properties were determined by performing a geometry optimization procedure, that involved evaluating the total energy per unit cell across various values of the lattice constants. The optimization process involved minimizing the total energy with respect to the lattice parameters and fitting the data to the Birch–Murnaghan equation of state [17] given by Eq. (1).

$$\Delta E(V) = BV_o\left[\left(\frac{V_n}{B'}\right) + \left(\frac{1}{1-B'}\right) + \left(\frac{V_n}{B' - (B' - 1)}\right)\right] \quad (1)$$

where $\Delta E(V) = E\text{-}E_0$, B is the bulk modulus, B' pressure derivative of the bulk modulus and V_0 is the equilibrium volume and E_0 equilibrium energy at zero pressure.

Trials were carried out by exchanging the Wyckoff positions for Zr, Co, and As, resulting in three samples illustrated in Table 1. The most energetically stable sample was considered for the rest of the calculations performed in this study. The optimized parameters were used to calculate the electronic, optical, elastic, and dynamic properties of ZrCoAs following the procedure described in Refs. [15,18]. For example, for the lattice dynamics, phonon dispersion was studied; Six two-dimensional super cells with a total of 24 atoms were created using a 3-atom unit cell, with one atom each of Zr, Co, and As. The Phonopy code [19] was used to calculate the phonons. Elastic constants were

Table 1
Wyckoff positions for the three possible configurations of ZrCoAs half Heusler alloy in space group number 216 and symbol F43 m.

Atomic configurations	Zr	Co	As
XYZ	4a(0,0,0)	4b(0.5,0.5,0.5)	4c (0.25,0.25,0.25)
ZXY	4c (0.25,0.25,0.25)	4a(0,0,0)	4b(0.5,0.5,0.5)
YZX	4b(0.5,0.5,0.5)	4c (0.25,0.25,0.25)	4a(0,0,0)

calculated using the Quantum ESPRESSO Thermo-PW post-processing code [20]. The Lagrangian theory of elasticity, in which a solid is considered to be an anisotropic and homogeneous elastic medium, was used to compute the elastic properties. Due to the cubic symmetry of ZrCoAs, there are three independent elastic constants stated in section III.C, these were computed using the Voigt, Reuss, and Hill averaging approach [21]. Elastic moduli were described as follows:

The bulk modulus B, which is the measure of resistance to compressibility, is calculated using the expression in Eq. (2).

$$B = \frac{1}{3}(C_{12} + 2C_{12}) \quad (2)$$

For Voigt, Reuss, and Hill averages, the bulk modulus for a cubic structure is the same. The Shear modulus, which is the deformation that occurs in a solid when a force is applied to one of parallel faces while the other face opposite the parallel face is held in place by opposing forces, is calculated for the cubical symmetry in the Voigt average using Eq. (3)

$$G_V = \frac{(C_{11} - C_{12} + 3C_{44})}{5} \quad (3)$$

The Reuss average is calculated using the expression presented in Eq. (4).

$$G_R = \frac{5(C_{11} - C_{12})C_{44})}{4C_{44} + 3(C_{11} - C_{12})} \quad (4)$$

The arithmetic mean of the Voigt and Reuss average in Eq. (5) gives the Hill shear modulus.

$$G_H = \frac{G_V + G_R}{2} \quad (5)$$

Eq. (6) and Eq. (7) are used to compute the Young's modulus and the Poisson's ratio

$$E = \frac{9BG}{(3B + G)} \quad (6)$$

$$\upsilon = \frac{3B - 2G}{2(3B + G)} \quad (7)$$

By replacing G with G_V and G_R in Eq. (6) and Eq. (7), the Voigt and Reuss averages of Young's modulus and Poisson's ratio are calculated. Eq. (8), is based on Debye's assumption that the temperature is the highest normal mode of vibration. Debye's temperature (θ_D) is determined as indicated in Eq. (8).

$$\theta_D = \frac{h}{k}\left[\frac{3n}{4\pi}\left(\frac{\rho N_A}{M}\right)\right]^{\frac{1}{3}} \mu_m \quad (8)$$

where, h is Planck's constant, k is Boltzmann's constant, N_A is the Avogadro's number, n is the number of atoms per molecule or per formula unit, M is the molar mass, ρ is the density of the unit cell and μ_m is the average sound velocity. Anisotropy (A), a physical characteristic that is related to elastic properties, was calculated using Eq. (9) to determine the type of bonding in various crystallographic directions.

$$A = \frac{2C_{44}}{C_{11} - C_{12}} \quad (9)$$

By comprehensively analyzing these properties, this study aims to shed light on the potential of ZrCoAs's suitability for photovoltaic applications. The results obtained from this research will contribute to the advancement of sustainable energy technologies, which addresses the global demand for clean and renewable energy sources.

3. Results and discussions

A. Structure of ZrCoAs

Geometry optimization of the ZrCoAs half-Heusler (HH) compound was carried out by calculating the lattice parameter as a function of the total energy. To determine structural stability from an energy point of view, the formation energy ($E^{formation}$) of the ZrCoAs compound was calculated using Eq. (10);

$$E^{formation} = E^{total}(ZrCoAs) - \left[E^{Zr} + E^{Co} + E^{As}\right] \quad (10)$$

Where E^{Zr}, E^{Co}, and E^{As} are energy per atom for bulk Zr, Co and As, respectively. The tests were carried out by exchanging the Wyckoff positions for Zr, Co and As, resulting in three samples shown in Table 1.

The most energetically stable sample (YXZ), as indicated in Fig. 1, has its atoms at the Wyckoff positions 4b(0.5,0.5,0.5), 4c (0.25,0.25,0.25), and 4a(0,0,0) for Zr, Co, and As, respectively. This configuration is consistent with the findings of Osafile et al. [22]. Therefore this sample is deemed the most preferred and was used for subsequent calculations. The optimized structure of the YXZ sample, shown in Fig. 2, has lattice parameters a = b = c and angles $\alpha = \beta = \gamma = 90^0$.

Using the formula in Eq. (10), a formation energy of −2.69 eV was obtained for the most energetically stable sample YXZ. The negative result means that energy is gained during the formation process, suggesting not only structural stability, but also potential experimental feasibility for the alloy. The Zr–Co bond length, calculated at 2.64 Å, is equal to the Co–As bonds but slightly shorter than the Zr–As bonds (3.05 Å). These calculated bond lengths align well with those reported for similar Zr-based HH compounds by Allan et al. (2023) [18], indicating a precise definition of the structure.

Fig. 2b and c, respectively, show the lattice constant (a_0) and the energy relationship. Subsequently, the obtained data from the energy-lattice parameter relationship were fitted to the Birch-Murnaghan equation of state (Eq. (1)). The ground state properties of ZrCoAs after the fitting process yielded a lattice parameter of a = 6.0238 Å and 5.954 Å respectively, without and with SOC effects. Additional ground-state properties obtained from the fitting are listed in Table 2.

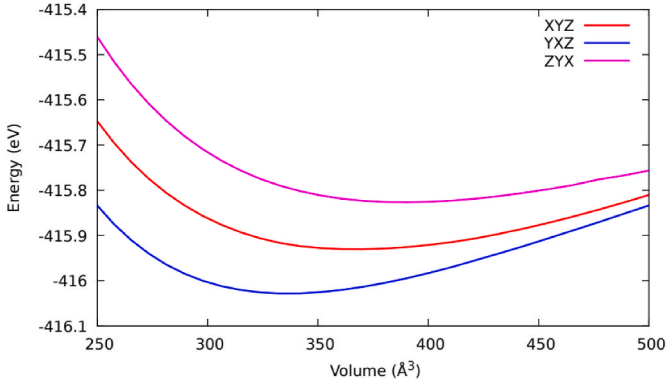

Fig. 1. Total energy against the Volume for the three possible configurations, showing the most energetically favoured atomic configuration for cubic ZrCoAs.

As illustrated in Table 2, the calculated bulk modulus of 143.7 GPa and the lattice constant is 6.023 Å for ZrCoAs without SOC are obtained, which are in accordance with the reported values for ZrCoSb and ZrCoBi [18]. The bulk modulus is a measure of a material's resistance to compression or volume change under pressure. A higher bulk modulus indicates greater stiffness and a more compact structure. In this case, ZrCoAs has the highest bulk modulus compared to the other Zr- based HH compounds considered in Table 2. The volume of ZrCoAs is approximately 49.75 $Å^3$ without SOC and 49.66 $Å^3$ with SOC, which is consistent with what was achieved for ZrCoSb and ZrCoBi in Ref. [18]. The volume represents the size of the unit cell and provides information about the density of the material. In this case, ZrCoAs have the largest volume among the three materials. For the minimum energy (Emin) and electronic band gaps, ZrCoAs has Emin of −5660.23 eV without SOC and −5593.84 eV with SOC. The corresponding band gap for ZrCoAs is 1.09 eV without SOC and 0.85 eV with SOC. This is in good agreement with the reported results for ZrCoSb and ZrCoBi. The minimum energy (Emin) represents the equilibrium energy of the material, and the band gap indicates the energy range between the highest-occupied and lowest-unoccupied electronic states. The significance and nature of the band gaps will be discussed in section III.B.

B. Electronic properties

To gain insight into the electronic bandgap size of ZrCoAs, electronic structure calculations were performed along the Γ-X-K-Γ-L-W-X high symmetry points [23], with and without SOC. From Fig. 3a, an indirect W symmetry point (conduction band minima) and the L symmetry point (valence band maxima) without SOC effects are observed. Fig. 4a confirms the indirect gap, located between the symmetry point Γ (minima of the conduction band) and the symmetry point L (maxima of the valence band) with SOC effects. When SOC is not included, ZrCoAs exhibit a band gap of 1.09 eV. However, when SOC is incorporated, the band gap reduces to 0.85 eV. This reduction in the band gap is attributed to the spin-orbit splitting caused by SOC. Spin-orbit coupling introduces energy corrections based on the interaction between the electron spin and its orbital motion, leading to a splitting of energy levels. In the presence of SOC, the energy bands near the band edges shift differently for spin-up and spin-down electrons, breaking the spin degeneracy and modifying the electronic structure as seen in Fig. 4a. The SOC-induced band splitting results in a change in the magnitude of the band gap, thereby decreasing it. Even though the material retains its indirect bandgap nature, the position of the Valence Band Maxima and Conduction Band Minimum changes, an indication that the SOC effect enhances the overlap between the valence and conduction bands, making the material more favorable for certain electronic and optoelectronic applications [24,25].

It is therefore important to consider the SOC effect when studying and designing devices based on ZrCoAs, especially those that rely on its electronic properties, such as solar cells, transistors, or other energy-harvesting and electronic devices. SOC can significantly influence the behavior and functionality of the material, making its accurate inclusion in simulations and calculations crucial for a comprehensive understanding of the electronic properties of ZrCoAs.

Further analysis of the density of states with SOC effects demonstrated how different states of the constituent elements contribute to the formation of the conduction and valence bands of the compound. In Fig. 3b, it is evident that the formation of the valence band is predominantly influenced by the Co 3d and Zr 3d states, with the As 2p states making minimal contributions around the Fermi level (E_F) when SOC was not included in the calculation. In contrast, the formation of the conduction band is mainly attributed to the Zr 8d states, along with additional states from Co5d and As 3p when SOC is incorporated. The change in dominant states that contributes to the valence and conduction bands of ZrCoAs when SOC is incorporated in the electronic structure calculations can be attributed to the relativistic effects

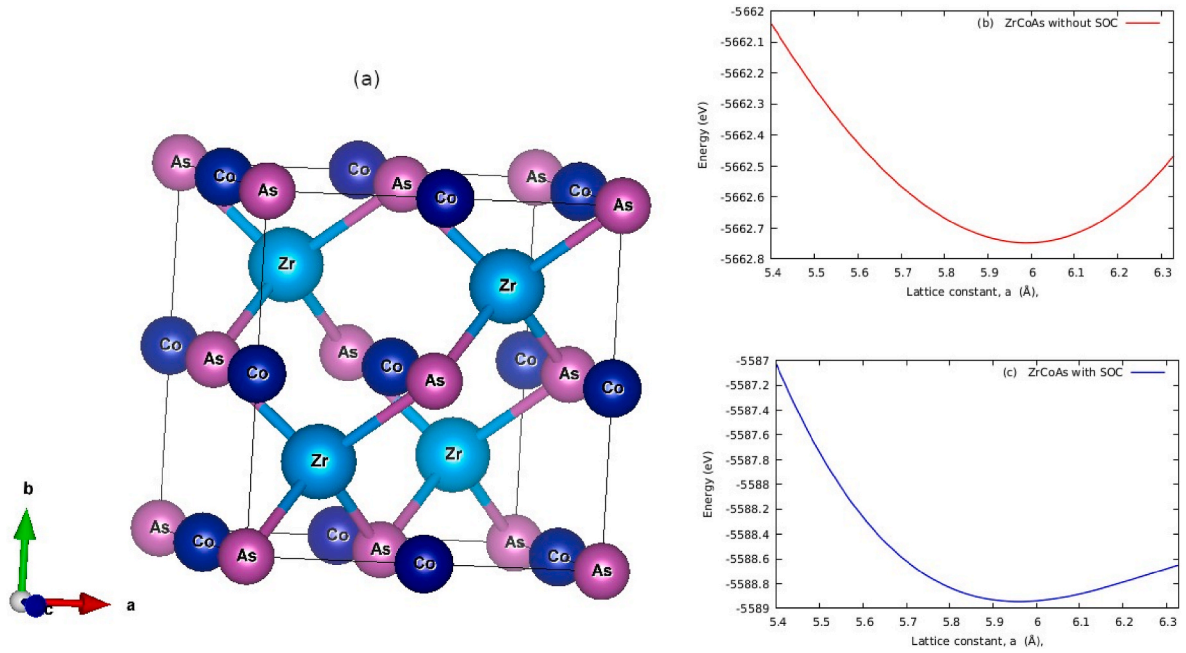

Fig. 2. (a) Optimized structure (b) Energy vs lattice constant curve without SOC, and (c) Energy vs lattice constant curve with SOC for cubic ZrCoAs.

Table 2
Lattice constants, its derivatives and electronic bandgap of ZrCoAs compared to similar Zr based half Heusler compounds.

Comp	Calculated bulk modulus (B in GPa)		a_0(Å)	Volume (Å)^3	Emin (eV)	Band gaps (eV)	Ref
	Birch -Murnaghan EoS	Thermo-pw					
ZrCoAs	143.7	107.9	6.023	49.75	−5660.23	1.0957	This work without SOC
ZrCoAs	145.7	107.9	5.954	49.66	−5593.84	0.85	This work with SOC
ZrCoSb	127.6	133.3	6.109	45.01	−7928.71	1.0765	Ref [18]
ZrCoBi	114.8	207.6	6.199	46.25	−7932.11	1.0416	Ref [18]

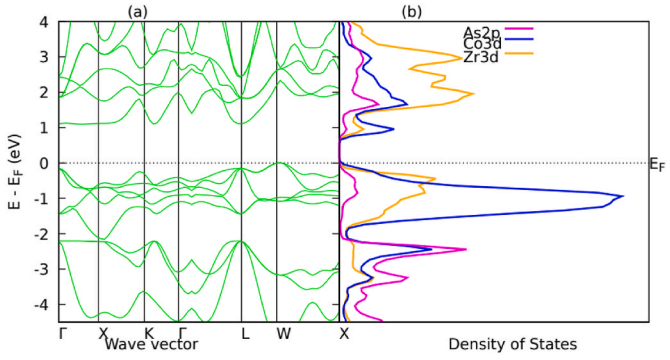

Fig. 3. plots for (a) Electronic band structure without SOC effects (b) density of states without SOC as a function of energy for ZrCoAs.

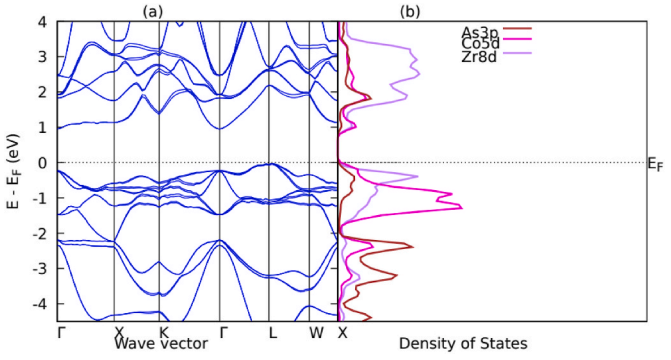

Fig. 4. Plots for (a) Electronic band structure with SOC, and (b) density of states with SOC as a function of energy for ZrCoAs.

introduced by SOC. Without SOC, the electronic structure calculations consider only the static interactions between the electrons and the atomic nuclei, neglecting the relativistic effects caused by the electron's motion relative to the atomic nucleus and its own spin. In this case, the dominant states influencing the valence and conduction bands are mainly determined by the 3d orbitals of cobalt (Co) and zirconium (Zr) atoms for the valence band and the 4d orbitals of zirconium (Zr) atoms for the conduction band. However, when SOC is incorporated into the calculations, the relativistic effects become significant. SOC considers the coupling between the electron's orbital motion and its intrinsic spin angular momentum because of the electron's charge and mass. This relativistic effect leads to spin-orbit splitting, which means that the energy levels of the electronic states are affected differently for electrons with different spin orientations. As a result of SOC, the contribution of additional atomic orbitals becomes more pronounced. In the conduction band, in addition to the dominant contribution from Zr 4d states, the Co 5d and As 3p orbitals also play a more substantial role. SOC-induced splitting modifies the electronic states near the edge of the band, causing these additional orbitals to contribute to the formation of the conduction band. The relativistic effects of SOC also impact the valence band, where the contributions of Co 3d and Zr 3d states remain dominant, but the As 2p states contribute minimally around the Fermi level (E_F). The subsequent spin up and spin down is calculated and presented in Fig. 5.

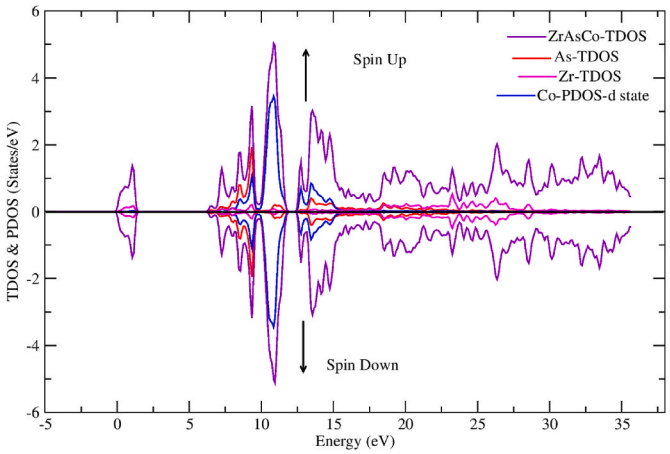

Fig. 5. Computed total and partial spin-polarized DOS for ZrCoAs.

Furthermore, the symmetric DOS, coupled with a higher total DOS, signifies a balanced distribution of energy states conducive to efficient charge transport. In the realm of photovoltaics, this characteristic is desirable for optimizing the absorption of sunlight and promoting effective electron-hole pair generation [27]. The absence of spin asymmetry simplifies the material's behavior, making it potentially more suitable for integration into photovoltaic devices where the efficiency of charge separation and transport is crucial.

Overall, the inclusion of SOC in the electronic structure calculations alters the electronic band structure by introducing spin-orbit splitting, which changes the dominant atomic orbitals that contribute to the valence and conduction bands of ZrCoAs. SOC provides a more accurate description of the electronic properties, especially in materials with heavy elements and strong spin-orbit coupling interactions, like ZrCoAs. Given this, the SOC effects were incorporated into the rest of the calculations in this study. Furthermore, Table 2 compares the band gap with those of selected ZrCoSb/Bi compounds. To determine which material is the most favorable for solar energy harvesting, we need to consider the band gap of the material and its compatibility with solar energy conversion processes. In solar energy harvesting, materials with appropriate band gaps that can efficiently absorb solar photons and generate charge carriers (electrons and holes) are preferred [28]. A suitable band gap allows the material to absorb a significant portion of sunlight and enables efficient energy conversion. Based on the band gaps reported and calculated in Table 2, we can compare the band gaps of the materials. ZrCoAs (both with and without SOC) have the widest band gap, which means that they require photons with higher energy (shorter wavelengths) to be efficiently absorbed. On the other hand, ZrCoSb and ZrCoBi have slightly narrower band gaps, making them capable of absorbing a broader range of solar photons. In solar energy harvesting, it is generally more favorable to have a material with a band gap close to the optimal value for solar absorption, which is around 1.1–1.4 eV. This range corresponds to the energy of visible light, where a significant portion of solar radiation lies [29].

In Fig. 5, it is observed that the density of states (DOS) configuration in ZrCoAs is symmetric, where the pat-tern remains exactly the same on both sides of spin up and spin down. This adds a layer of significance to its potential applications in photovoltaics. This symmetry implies a spin degeneracy, indicating that the energy levels for electrons with opposite spin orientations are identical. In the context of photovoltaics, a symmetric DOS is advantageous as it suggests a lack of strong spin-dependent effects that could lead to unwanted electronic complications. This implies a simplified electronic structure, facilitating a more predictable and controllable behavior of charge carriers during the conversion of solar energy [26].

However, it is important to note that the analysis of the material's electronic properties is just one factor, and other material properties and engineering considerations may also play a role in determining the overall performance and efficiency of a solar energy harvesting device. Also, the Kohn-Sham DFT is well known to underestimate the electronic band gaps [30]. Among the optical properties calculated of ZrCoAs in section III E, the optical gap will be discussed.

C. Elastic and Mechanical Stability

The crystal structure of the half-Heusler compound ZrCoAs is characterized by a face-centered cubic arrangement. Within the cubic crystal system, there are three independent elastic constants, namely C_{11}, C_{12}, and C_{44} [31]. The calculated values for these elastic constants were found to be $C_{11} = 180.07$ GPa, $C_{12} = 26.8$ GPa, and $C_{44} = 71.13$ GPa, indicating that the ZrCoAs semiconductor is mechanically stable according to Born's criteria [32]. The derived values using the Voigt–Reuss–Hill approximation for bulk modulus (B), Young's modulus (E), shear modulus (G), and Poisson's ratio (v) as presented in Table 4. The Pugh ratio (B/G) of 1.47 indicates that the material is ductile. Additionally, Poisson's ratio (v), a mechanical property of materials that represents the ratio of lateral strain to axial strain when a material is subjected to uniaxial stress, is a dimensionless quantity that characterizes a material's response to deformation in different directions [33]. From our calculations, Poisson's ratio suggests that the compound exhibits ionic properties. Their results are in good agreement with the reported Zr-based half Heusler alloys tabulated in Table 4.

Fig. 6 shows the degree of anisotropy dependence on the deviation of a geometrical body from the spherical shape. In this case, the representation is in a 2D shape. If a geometric body is of spherical (3D) or circular (2D) shape, it exhibits isotropy, which is observed in all planes for Young's modulus, shear modulus, and Poisson's ratio at slightly different degrees. The degree of anisotropy is observed to be symmetric for Young's modulus, shear modulus, and Poisson's ratio. The anisotropic variation for the calculated values of Young's modulus, the shear modulus, and Poisson's ratio are tabulated in Table 3.

Table 3 provides a comprehensive view of the material properties of ZrCoAs, a crucial endeavor to understand their mechanical behavior. Three different averaging schemes, Voigt, Reuss, and Hill, offer consistent estimates for the bulk modulus, Young's modulus, shear modulus, and Poisson's ratio. In particular, the bulk modulus values are strikingly uniform at approximately 107.9 GPa in all schemes, indicating that ZrCoAs possess robust resistance to volume changes when subjected to external pressure. Likewise, the values for Young's modulus, ranging from roughly 167.29 GPa–167.46 GPa, show a high degree of stiffness and elasticity, making ZrCoAs well-suited for applications requiring load-bearing capacity. The shear modulus values, around 73.23 GPa–73.33 GPa, further confirm its strength to resist shear deformation. Despite minor variations, Poisson's ratio values (ranging from 0.1418 to 0.14216) indicate consistent behavior in response to different types of stress. This behavior is confirmed in Fig. 6. The remarkable consistency in the estimated values suggests that ZrCoAs can be classified as an isotropic material, making it ideal for engineering applications where uniform mechanical behavior is essential.

Eigenvalues are fundamental in solid mechanics, because they describe the stiffness properties of materials, allowing researchers and engineers to comprehend how a material responds to external forces and deformations. As illustrated in Table 5, these eigenvalues signify

Table 3
Average properties of ZrCoAs.

Averaging scheme	Bulk modulus (GPa)	Young's modulus (GPa)	Shear modulus (GPa)	Poisson's ratio
Voigt	107.9	167.46	73.33	0.1418
Reuss	107.9	167.29	73.23	0.14216
Hill	107.9	167.37	73.28	0.14198

Table 4
The derived values using the Voigt-Reuss-Hill approximation for bulk modulus (B), Young's modulus (E), shear modulus (G), Debye's Temperature θ_D, and Poisson's ratio (v).

Comp	C_{11}	C_{12}	C_{44}	B(GPa)	G(GPa)	B/G	E(GPa)	v	θ_D (K)	REF
ZrCoAs	180.1	26.8	71.1	107.9	73.2	1.47	167.3	0.14	403.39	This work
ZrCoSb	262.3	68.1	67.7	113.3	79.9	1.66	199.8	0.25	393.12	Ref [18]
ZrCoBi	322.2	150.3	52.7	207.6	64.3	3.23	174.7	0.35	312.75	Ref [18]

different stiffness characteristics of ZrCoAs in various directions. It is worth noting that the eigenvalues λ_1, λ_2, and λ_3 are the same (711.36 GPa), indicating that ZrCoAs has an isotropic behavior in these directions. In contrast, λ_4, λ_5, and λ_6 are different, suggesting different stiffness characteristics in other directions.

Young's modulus, with a minimum of 163.61 GPa and a maximum of 173.12 GPa, as illustrated in Table 6, indicates that ZrCoAs can withstand mechanical stresses and deformations. In particular, the maximum value of Young's modulus suggests the potential of ZrCoAs as a resilient material for use in photovoltaic applications. Furthermore, the uniformity of the linear compressibility values (0.42782 TPa^{-1} for both minimum and maximum) means that ZrCoAs can maintain consistent volume stability under varying environmental conditions, an attribute essential for solar panel materials that must withstand changes in temperature and pressure.

The Shear Modulus values, ranging from 71.13 GPa (minimum) to 76.62 GPa (maximum), are relevant in the case where materials need to withstand shear forces caused by wind loads. The capability of ZrCoA to resist shearing deformations makes it a promising candidate for use in the mechanical components of solar tracking systems. However, the Poisson ratio values are essential in understanding how a material responds to different strains. The range of these values, as tabulated in Table 6, shows the ability of ZrCoAs to adapt to varying stress and strain conditions, which is invaluable for materials used in solar panels that experience different mechanical loads, including thermal expansion and contraction.

D. Dynamical Stability

Lattice dynamics is the study of how the atoms in a crystal lattice vibrate and interact with each other [34–36]. The phonon dispersion and Density of States (DOS) are key components of lattice dynamics analysis and provide valuable insights into the thermal and vibrational behavior of materials like ZrCoAs. The phonon dispersion curve obtained for ZrCoAs represents the relationship between phonon frequencies and wavevectors in the Brillouin zone as shown in Fig. 7a.

The different branches of the dispersion curve correspond to various phonon modes, and the dispersion along each branch provides information about the vibrational properties of the material [37]. In Fig. 7a at the Γ point of the Brillouin zone, there are three acoustic phonon modes, one for each crystallographic direction. These modes have low frequencies and correspond to the collective vibrations of atoms in the crystal lattice. They play a crucial role in determining the thermal conductivity of the material, as they carry heat energy through lattice vibrations [37]. On the other hand, the optical phonon modes are higher in frequency and correspond to vibrations that involve the relative motion of atoms within the unit cell [37]. Fig. 7b shows the density of states (DOS) plot, which shows the distribution of the phonon states with respect to their energies. It provides information on the number of phonon modes that are available at different energy levels. The peaks in the DOS curve represent the allowed phonon modes, and the area under the curve corresponds to the total number of phonon states. The phonon frequencies and modes dictate the vibrational behavior of the material. The presence of specific phonon modes can give rise to characteristic vibrational patterns, influencing various properties. In this study, the phonon branches near the Brillouin zone boundaries are of particular interest. These modes are associated with specific lattice distortions and can give insight into the stability and mechanical properties of ZrCoAs. For example, soft-phonon modes near the Brillouin zone boundary indicate a phase transition or structural instability. Additionally, the absence of negative frequencies is a clear indication that the ZrCoAs are dynamically stable. The lattice dynamics analysis based on the phonon dispersion and DOS for ZrCoAs provides an understanding of its vibrational and thermal properties, which are crucial in designing and optimizing the material for various technological applications, such as thermoelectric and optoelectronic devices.

E. Optical Properties

The optical properties of ZrCoAs, which are essential for understanding its suitability for optoelectronic and photovoltaic applications, are reported in this section. The complex dielectric function was used to determine properties such as refractive index (n), extinction coefficient (k), absorption coefficient (α) and energy loss (L). The dielectric constant (ε) is a complex property characterizing how materials respond to electric fields. It consists of real (ε_1) and imaginary (ε_2) parts. The dielectric constant is expressed as $\varepsilon = \varepsilon_1 + i\varepsilon_2$. The real part ($\varepsilon$) reflects a material's polarizability indicating its ability to store electrical energy. The imaginary part (ε_2) relates to energy dissipation and losses, demonstrating how much energy is absorbed and converted into other forms, such as heat [38]. The frequency-dependence behavior of $\varepsilon 2$ (ω) reveals resonances associated with molecular or atomic structures. Together, these components provide a comprehensive understanding of the electrical behavior of a material, which is crucial for designing efficient electronic devices. The results are presented in Fig. 8, Figs. 9 and 10 summarized in Table 7.

In Fig. 7, the main peaks in the complex dielectric functions are observed between 1.9 eV and 4.5 eV, with additional peaks at 6.1 eV and 7.3 eV. Regions where $\varepsilon_1(\omega) < 0$ indicated that incident photons are fully attenuated. The refractive index and extinction coefficient, illustrated in Fig. 8, are obtained from the dielectric functions. They provide valuable information about the optical behavior of the material [39,40]. In Fig. 9, ZrCoAs is a good absorber of photon energy with very minimal energy loss.

Based on the results reported in Table 7, ZrCoSb has the lowest optical bandgap indicating that it is more efficient in absorbing a wider range of solar photons compared to ZrCoAs with a bandgap of 1.78 eV. However, both ZrCoSb and ZrCoBi have been reported to have refractive indices compared to the calculated refractive index of ZrCoAs (2.560), suggesting better light bending and trapping abilities suitable for light management in solar energy harvesting applications [28]. The optical properties of ZrCoAs are comparable to those of the other reported Zr-based HH compounds.

4. Conclusion

In conclusion, the comprehensive study of ZrCoAs has provided valuable information on its structural, electronic, optical, dynamical, elastic, and mechanical properties. The compound exhibits a stable crystal structure, which makes it promising for practical applications. Electronic band structure analysis indicates contributions primarily from Co 3d and Zr 3d states, influencing the material's electronic behavior with an indirect bandgap of 1.0957 eV without SOC and 0.85 eV with SOC, suggesting its potential for solar energy harvesting and

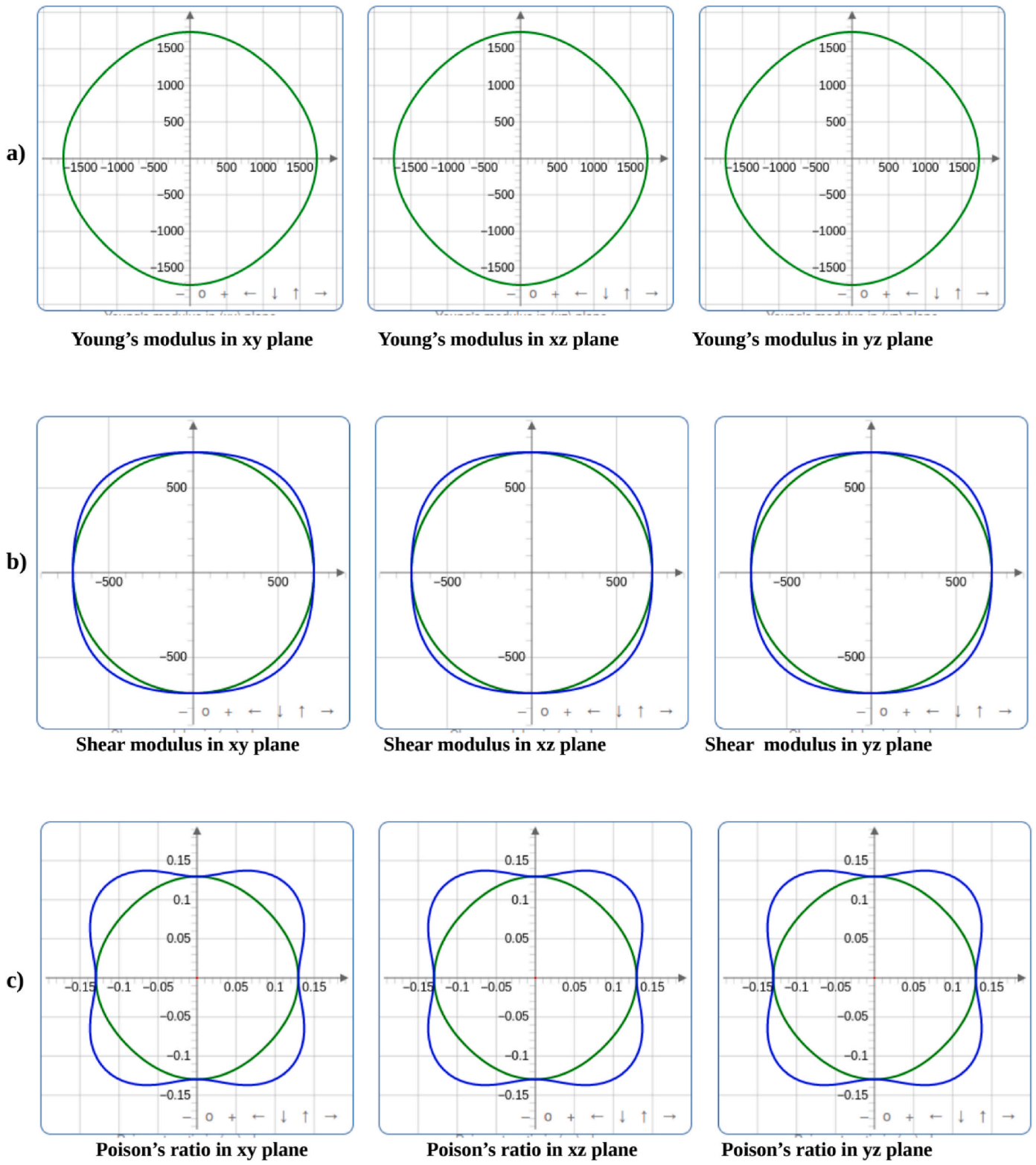

Fig. 6. The spatial dependency of (a) Young's modulus, (b) Shear modulus, and (c) Poisson's ratio for ZrCoAs, (Blue and green indicate the maximum and minimum values, respectively).

Table 5
Eigenvalues of the stiffness matrix for ZrCoAs in GPa.

$\lambda 1$	$\lambda 2$	$\lambda 3$	$\lambda 4$	$\lambda 5$	$\lambda 6$
711.36	711.36	1532.4	1532.4	1532.4	2337.4

optoelectronic applications. The lattice dynamical analysis reveals phonon frequencies and modes, contributing to thermal and vibrational behavior, with particular interest in phonon branches near the Brillouin zone boundaries. In terms of mechanical properties, ZrCoAs exhibit Young's modulus of 167.3 GPa, a shear modulus of 73.2 GPa, and a bulk modulus of 107.9 GPa, indicating its mechanical strength and resistance

Table 6
Variations of the elastic moduli for ZrCoAs.

	Young's modulus		Linear compressibility		Shear modulus		Poisson's ratio	
	Emin	*Emax*	*βmin*	*βmax*	*Gmin*	*Gmax*	*vmin*	*vmax*
Value	163.61 GPa	173.12 GPa	0.42782 TPa^{-1}	0.42782 TPa^{-1}	71.13 GPa	76.62 GPa	0.12428	0.16602
Anisotropy	1.058		1.0000		1.077		1.3359	

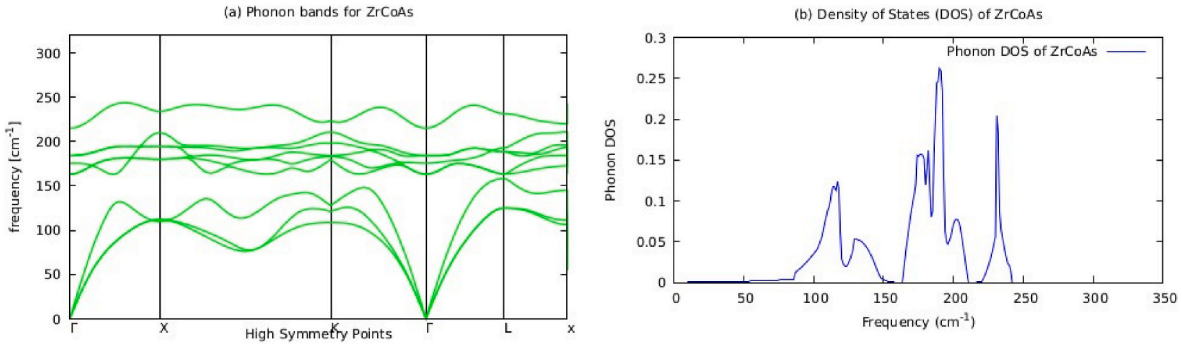

Fig. 7. Plots for (a) Phonon band structure, and (b) phonon density of states (DOS) for ZrCoAs.

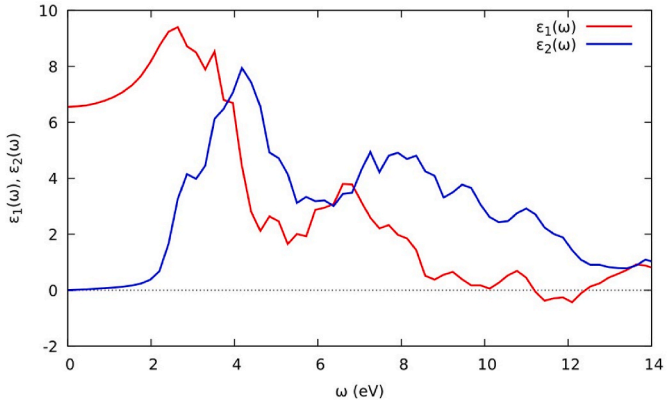

Fig. 8. Frequency-dependent complex dielectric functions $\varepsilon_1(\omega)$ and $\varepsilon_2(\omega)$.

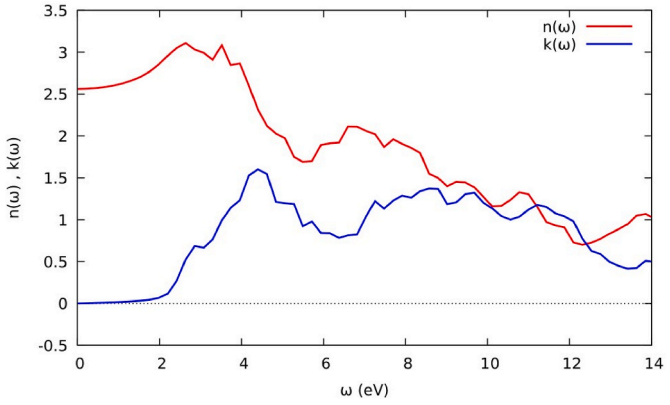

Fig. 9. Frequency-dependent refractive index n(ω) and extinction coefficient k(ω).

to deformation. The material's B/G ratio of 1.47 suggests its ability to withstand volume changes compared to shear deformation. Additionally, ZrCoAs has a relatively low Poisson ratio of 0.14, indicating its limited lateral contraction under tensile stress. The optical properties of ZrCoAs are excellent for photovoltaic applications, indicating potential

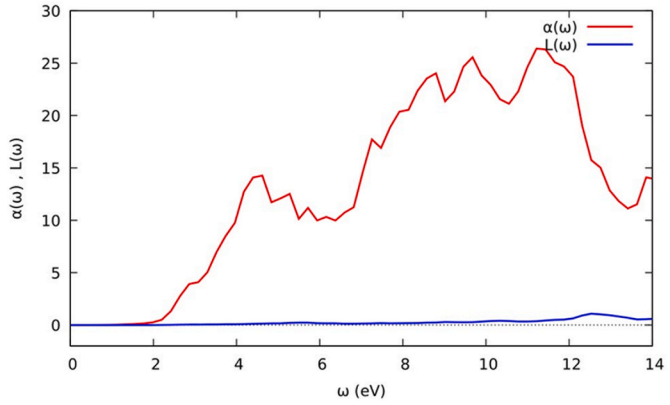

Fig. 10. Frequency-dependent absorption coefficient α (ω) and energy loss L(ω).

Table 7
Optical properties of ZrCoAs compared to selected Zr-based half Heusler compounds.

Comp	$\varepsilon_1(0)$	ΔE_{OG}	$n(0)$	$R(0)$	$L(0)$	Ref
ZrCoAs	22.67	1.78	2.560	0.19205	0.000352	This work
ZrCoSb	19.7	1.36	4.435	0.399	0.000347	Ref [18]
ZrCoBi	21.1	1.55	4.593	0.413	0.000344	Ref [18]

for use in solar energy harvesting devices. Its optical properties are comparable to those of the other two reported Zr-based HH compounds, ZrCoSb and ZrCoBi. Overall, the collective investigation of these properties provides a comprehensive understanding of ZrCoAs, offering opportunities for optimizing its performance in various technological applications. These insights contribute to the potential use of ZrCoAs in solar cells, optoelectronic devices, thermoelectric applications, and structural components, promoting advancements in the fields of renewable energy and materials science. As researchers continue to explore and harness the potential of ZrCoAs, it holds promise in contributing to advances in renewable energy technologies and materials science because of its versatility and suitability for a wide range of practical applications.

CRediT authorship contribution statement

Lynet Allan: Conceptualization, Formal analysis, Methodology, Writing – original draft. **R.E. Mapasha:** Conceptualization, Supervision, Writing – review & editing. **Winfred M. Mulwa:** Formal analysis, Supervision, Validation, Writing – review & editing. **Julius M. Mwabora:** Formal analysis, Supervision, Validation. **Robinson J. Musembi:** Supervision, Validation, Formal analysis.

Declaration of competing interest

The authors declare that they have no known competing financial interests or personal relationships that could have appeared to influence the work reported in this paper.

Data availability

Data will be made available on request.

Acknowledgment

The authors gratefully acknowledge the invaluable support of the Partnership for Skills in Applied Sciences, Engineering, and Technology (PASET)-Regional Scholarship Innovation Fund (RSIF), which provided additional funding through the DOCTAS Grant. This grant was made possible through a collaborative partnership between icipe, RCU, and the Carnegie Corporation of New York (CCNY). The authors also express their appreciation to the Center for High-Performance Computing (CHPC) at RSA for providing essential computing resources crucial for the computational simulations and analyses in this research. The University of Pretoria is acknowledged for its support.

References

[1] O. Tahvonen, S. Salo, Economic growth and transitions between renewable and nonrenewable energy resources, Eur. Econ. Rev. 45 (8) (2001) 1379–1398.
[2] T. Graf, S.S. Parkin, C. Felser, Heusler compounds—a material class with exceptional properties, IEEE Trans. Magn. 47 (2) (2010) 367–373. https://ieeexplore.ieee.org/abstract/document/5654590/.
[3] T. Nadjia, et al., Theoretical prediction of structural, magnetic and electronic properties of a New SiRbCa heusler alloy, Chemistry Africa (2023) 1–10.
[4] L. Drici, et al., First-principles calculations of structural, elastic, electronic, and optical properties of CaYP (Y= Cu, Ag) Heusler alloys, Emergent Materials (2022) 1–16.
[5] S. Ullah, et al., First-principles calculations to investigate optical properties of topological semimetal MX compounds (M= Ti, Zr, Hf and X= S, Se, Te), Mater. Today Commun. 35 (2023) 106001.
[6] A. Saim, et al., Investigation of the structural, elastic, electronic, and optical properties of half-heusler CaMgZ (Z= C, Si, Ge, Sn, Pb) compounds, J. Electron. Mater. 51 (7) (2022) 4014–4028.
[7] N. Chami, et al., Computational prediction of structural, electronic, elastic, and thermoelectric properties of FeV X (X= as, P) half-heusler compounds, J. Electron. Mater. 49 (2020) 4916–4922.
[8] B. Asma, et al., Structural, mechanical, magnetic, electronic, and thermal investigations of Ag2YB (Y= Nd, Sm, Gd) full-Heusler alloys, Emergent Materials 4 (6) (2021) 1769–1783.
[9] T. Graf, C. Felser, S.S. Parkin, Simple rules for the understanding of Heusler compounds, Prog. Solid State Chem. 39 (1) (2011) 1–50. https://www.sciencedirect.com/science/article/pii/S0079678611000021.
[10] L. Samia, et al., Investigation of structural, elastic, electronic, and magnetic proprieties for X2LuSb (X= Mn and Ir) full-Heusler alloys, Emergent Materials 5 (2) (2022) 537–551.
[11] D. Chattaraj, S. Dash, C. Majumder, Structural, electronic, elastic, vibrational and thermodynamic properties of ZrNi and ZrNiH3: a comprehensive study through first principles approach, Int. J. Hydrogen Energy 41 (44) (Nov. 2016) 20250–20260, https://doi.org/10.1016/j.ijhydene.2016.09.046.
[12] A. Jain, et al., Commentary: the Materials Project: a materials genome approach to accelerating materials innovation, Apl. Mater. 1 (1) (2013) 011002 [Online]. Available: https://aip.scitation.org/doi/10.1063.
[13] L. Talirz, et al., Materials Cloud, a platform for open computational science, Sci. Data 7 (1) (2020) 1–12 [Online]. Available, https://scholar.googleusercontent.com/scholar.bib?q=info:7a2oXMCiqkkJ:scholar.google.com/&output=citation&scisdr=CgVAeMUUEODwnOY1R3k:AAGBfm0AAAAAY34zX3mZg-xDb_isclxjTmw-MxZsPutG&scisig=AAGBfm0AAAAAY34zX2ROAjMsOuesV-lG-7ET9nxz17n9&scisf=4&ct=citation&cd=-1&hl=en.
[14] J.P. Perdew, K. Burke, M. Ernzerhof, Generalized gradient approximation made Simple, Phys. Rev. Lett. 77 (18) (Oct. 1996) 3865–3868, https://doi.org/10.1103/PhysRevLett.77.3865.
[15] L. Allan, W.M. Mulwa, R. Mapasha, J.M. Mwabora, R.J. Musembi, First principle study of ATiO 3 (A= Ti, Sr) materials for photovoltaic applications, J. Mol. Model. 30 (2) (2024) 32.
[16] G. Kresse, D. Joubert, From ultrasoft pseudopotentials to the projector augmented-wave method, Phys. Rev. B 59 (3) (Jan. 1999) 1758–1775, https://doi.org/10.1103/PhysRevB.59.1758.
[17] V. Tyuterev, N. Vast, Murnaghan's equation of state for the electronic ground state energy, Comput. Mater. Sci. 38 (2) (2006) 350–353 [Online]. Available: https://www.sciencedirect.com/science/article/pii/S0927025606000735.
[18] L. Allan, W.M. Mulwa, J.M. Mwabora, R.J. Musembi, E. Mapasha, An Ab-Initio Study of P-type Zrcoy (Y = Sb and Bi) Half - Heusler Semiconductors, May 2023, https://doi.org/10.2139/ssrn.4443887.
[19] A. Togo, First-principles phonon calculations with phonopy and phono3py, J. Phys. Soc. Jpn. 92 (1) (2023) 012001.
[20] T. Sekimoto, K. Kurosaki, H. Muta, S. Yamanaka, Thermoelectric and thermophysical properties of TiCoSb-ZrCoSb-HfCoSb pseudo ternary system prepared by spark plasma sintering, Mater. Trans. 47 (6) (2006) 1445–1448 [Online]. Available: https://www.jstage.jst.go.jp/article/matertrans/47/6/47_6_1445/_article/-char/ja/.
[21] P. Giannozzi, et al., Advanced capabilities for materials modelling with Quantum ESPRESSO, J. Phys. Condens. Matter 29 (46) (Oct. 2017) 465901, https://doi.org/10.1088/1361-648x/aa8f79.
[22] O. Osafile, J. Umukoro, Stability of X-IV-IV half Heusler semiconductor alloys: a DFT study, Mol. Phys. 119 (12) (2021) e1936249.
[23] R. Evarestov, V. Smirnov, Modification of the Monkhorst-Pack special points meshes in the Brillouin zone for density functional theory and Hartree-Fock calculations, Phys. Rev. B 70 (23) (2004) 233101.
[24] A.M. Boldin, Analysis of spin polarization in half-metallic heusler alloys, Macalester Journal of Physics and Astronomy 3 (1) (2015) 3 [Online]. Available: https://digitalcommons.macalester.edu/mjpa/vol3/iss1/3/.
[25] K. Choudhary, F. Tavazza, Convergence and machine learning predictions of Monkhorst-Pack k-points and plane-wave cut-off in high-throughput DFT calculations, Comput. Mater. Sci. 161 (2019) 300–308.
[26] R.-C. Xiao, Y. Jin, H. Jiang, Spin photovoltaic effect in antiferromagnetic materials: mechanisms, symmetry constraints, and recent progress, Apl. Mater. 11 (7) (2023).
[27] O. Entin-Wohlman, R. Shekhter, M. Jonson, A. Aharony, Photovoltaic effect generated by spin-orbit interactions, Phys. Rev. B 101 (12) (2020) 121303.
[28] A. Zahedi, Maximizing solar PV energy penetration using energy storage technology, Renew. Sustain. Energy Rev. 15 (1) (2011) 866–870.
[29] Q. Jiang, R. Wan, Z. Zhang, Y. Lei, G. Tian, First-principles calculations to investigate Zr substitution enhanced thermoelectric performance of p-type ZrxHf1-xCoBi (x= 0, 0.25, 0.5, 0.75, 1) compounds, Phys. Lett. 424 (2022) 127839 [Online]. Available: https://www.sciencedirect.com/science/article/pii/S0375960121007039.
[30] E.S. Goh, J.W. Mah, T.L. Yoon, Effects of Hubbard term correction on the structural parameters and electronic properties of wurtzite ZnO, Comput. Mater. Sci. 138 (2017) 111–116.
[31] J. Pokluda, M. Černỳ, M. Šob, Y. Umeno, Ab initio calculations of mechanical properties: methods and applications, Prog. Mater. Sci. 73 (2015) 127–158.
[32] M. Born, Thermodynamics of crystals and melting, J. Chem. Phys. 7 (8) (1939) 591–603 [Online]. Available: https://aip.scitation.org/doi/abs/10.1063/1.1750497.
[33] K. Radja, et al., Investigation of structural, magneto-electronic, elastic, mechanical and thermoelectric properties of novel lead-free halide double perovskite Cs2AgFeCl6: first-principles calcuations, J. Phys. Chem. Solid. 167 (2022) 110795.
[34] C. Çoban, Y.Ö. Çiftçi, K. Çolakoğlu, Structural, electronic, elastic, optical, and vibrational properties of HfXSb (X= Co, Rh, Ru) half-Heusler compounds: an ab initio study, Indian J. Phys. 90 (11) (2016) 1233–1241 [Online]. Available: https://link.springer.com/article/10.1007/s12648-016-0873-2.
[35] C. Çoban, K. Çolakoğlu, Y.Ö. Çiftçi, First principles study of the structural, mechanical, phonon, optical, and thermodynamic properties of half-Heusler (HH) compound NbFeSb, Phys. Scripta 90 (9) (2015) 095701.
[36] S. Califano, V. Schettino, N. Neto, S. Califano, V. Schettino, N. Neto, Lattice Dynamics, Springer, 1981.
[37] M.T. Dove, Introduction to the theory of lattice dynamics, École thématique de la Société Française de la Neutronique 12 (2011) 123–159.
[38] N. Alfryyan, et al., First-principles calculations to investigate structural, electrical, elastic and optical characteristics of BWF3 (W= S and Si) fluoroperovskites, Results Phys. 52 (2023) 106812.
[39] S. Radiman, M. Rusop, Investigation of structural and optical properties of In-doped AlSb nanostructures, Experimental and Theoretical NANOTECHNOLOGY (2023) 49–76.
[40] S. Alnujaim, et al., Density functional theory screening of some fundamental physical properties of Cs2InSbCl6 and Cs2InBiCl6 double perovskites, Eur. Phys. J. B 95 (7) (2022) 114.